

## The ALICE Inner Tracking System: commissioning and running experience

---

**Vito Manzari<sup>1</sup>**

*INFN Bari, Italy*

*on behalf of the ALICE Collaboration*

*E-mail: vito.manzari@cern.ch*

The Inner Tracking System (ITS) is the innermost detector of the ALICE experiment at the LHC, the closest to the beam axis and therefore one of the key detectors for tracking and vertexing capabilities. The ITS consists of three coaxial subsystems, surrounding the beam pipe, each one comprising two layers in different silicon technologies: the Silicon Pixel Detector (SPD), the Silicon Drift Detector (SDD) and the double-sided Silicon Strip Detector (SSD), innermost to outermost respectively. The number, position, granularity and technologies of the layers were optimized for efficient track finding and high impact-parameter resolution in the severe high-multiplicity environment expected for the central Pb-Pb collisions at LHC energy.

This paper presents the main results of the ITS commissioning with cosmic rays and the first experience with circulating beams. Meanwhile this proceedings was in preparation, the first ALICE physics paper was published in 2009 based on the very first proton-proton collisions at 450-450 GeV recorded with the ITS triggered by the SPD.

*VERTEX 2009 (18<sup>th</sup> workshop) – VERTEX 2009  
Veluwe, the Netherlands  
September 13-18, 20*

---

<sup>1</sup> Speaker

## 1. Introduction

ALICE (A Large Ion Collider Experiment) is a general-purpose heavy-ion detector at the CERN LHC which focuses on QCD, the strong interaction sector of the Standard Model. It is designed to address the physics of strongly interacting matter and the quark-gluon plasma at extreme values of energy density and temperature in nucleus-nucleus collisions. It allows a comprehensive study of hadrons, electrons, muons, and photons produced in the collision of heavy nuclei (Pb-Pb), up to the highest multiplicities anticipated at the LHC.

As the single dedicated heavy-ion experiment at the LHC, ALICE is addressing a broad range of observables. The ALICE design was driven by the physics requirements as well as by the experimental conditions expected in nucleus-nucleus collisions at the LHC. The most stringent design constraint is the extremely high particle multiplicity, which could be up to three orders of magnitude larger than in typical pp interactions at the same energy. The tracking was made particularly safe and robust by using mostly three-dimensional hit information with many points in a moderate field of 0.5 T provided by the large L3 solenoid magnet. This was achieved with a combination of very low material thickness to reduce multiple scattering at low  $pt$  and a large tracking lever arm of up to 3.5 m to guarantee a good resolution at high  $pt$ .

The main tracking detectors in the central barrel are the Inner Tracking System (ITS), a six-layer silicon vertex detector, and the Time-Projection Chamber (TPC).

The Inner Tracking System (ITS) [1] consists of six cylindrical layers of silicon detectors located at radii between 4 and 43 cm from the beam axis and covering the pseudo-rapidity range  $|\eta| < 0.9$  for all vertices located within the length of the interaction diamond ( $\pm 1\sigma$ , i.e.  $\pm 5.3$  cm along the beam direction).

The basic functions of the ITS are: localize the primary vertex with a resolution better than 100  $\mu\text{m}$ , reconstruct the secondary vertices from the decays of heavy flavour and strange particle decays, track and identify particles with momentum below 200 MeV/c, improve the impact parameter and momentum resolution for particles reconstructed by the TPC and reconstruct particles traversing dead regions of the TPC. The ITS therefore contributes to practically all physics topics addressed by the ALICE experiment, as discussed in detail in [2].

## 2. ITS overview

The six ITS layers surround the beam pipe at average radii 3.9, 7.6, 15, 24, 38 and 43 cm, respectively. The number, position and segmentation of the layers and the technology choices were optimized for efficient track finding and high impact-parameter resolution in the severe high-multiplicity environment expected for the central Pb-Pb collisions at LHC energy. In particular, the outer radius is determined by the necessity to match tracks with those reconstructed in the TPC, and the inner radius is the minimum allowed by the radius of the beam pipe. The high particle density expected in heavy-ion collisions at LHC (up to 50 particles per  $\text{cm}^2$  for the layer closest to the interaction point) and the required impact parameter resolution (better than 100  $\mu\text{m}$ ) have dictated the choice of silicon pixel detectors for the innermost two-layer sub-detector (SPD). The SPD has binary readout and also provides a

prompt (Fast-OR) trigger signal contributing to the L0 trigger. Two layers of silicon drift detectors form the intermediate sub-detector (SDD). At the larger radii, where the track density is expected to be below one particle per  $\text{cm}^2$ , two layers of double-sided silicon micro-strip detectors form the outermost detector (SSD). The SDD and SSD have analogue readout and therefore can be used for particle identification via  $dE/dx$  measurement in the non-relativistic ( $1/\beta^2$ ) region. This feature gives the ITS stand-alone capability as a low- $pt$  particle spectrometer.

The SPD, SDD and SSD comprise each 240, 260 and 1698 detector modules, respectively. The innermost SPD layer has a more extended pseudo-rapidity coverage ( $|\eta| < 1.98$ ) to provide a larger acceptance for the measurement of charged-particles multiplicity. The main parameters for each of the three detector types are summarized in Table 1.

**Table 1:** Main parameters of the three ITS sub-detectors

Layer	Detector	Radius (cm)	Length (cm)	Surface ( $\text{m}^2$ )	Channels	Spatial precision ( $\mu\text{m}$ )		Cell size ( $\mu\text{m}^2$ )	Max occupancy central Pb-Pb (%)	Power dissipation (W)	
						$r\phi$	$z$			Barrel	End-cap
1	SPD	3.9	28.2	0.21	9.8M	12	100	50x425	2.1	1.35k	30
2		7.6	28.2						0.6		
3	SDD	15.0	44.4	1.31	133k	35	25	202x294	2.5	1.06k	1.75k
4		23.9	59.4						1.0		
5	SSD	38.0	86.2	5.0	2.6M	20	830	95x40000	4.0	850	1.15k
6		43.0	97.8						3.3		

The momentum and impact parameter resolution for low-momentum particles are dominated by multiple scattering effects in the material of the detector; therefore the design of all three sub-detectors implements specific solutions to minimize the amount of material in the active volume. The SPD, SDD and SSD material budget contributions are 2.3%, 2.4% and 2.2% of a radiation length, respectively. The ALICE ITS has indeed the lowest material budget of the silicon inner tracker of the LHC experiments. The tracking capability is made particularly safe and robust in a large dynamic range by using mostly three-dimensional hit information in a moderate field of 0.5 T. This allows extending the dynamic range for the momentum measurement down to tens of MeV/c. The relative momentum resolution achievable with the ITS is better than 2% for pions with transverse momentum of 100 MeV/c [3].

For the ITS, the total dose expected during the lifetime of the experiment ranges from a few tens of Gy for the outer layers to about 2.7 kGy for the innermost SPD layer [1]. Deep-submicron radiation tolerant technologies have been used throughout the system for the front end electronics, and all components were tested for radiation hardness to levels exceeding significantly the expected radiation levels.

The main characteristics of the three sub-detectors are summarized hereafter, more details can be found in [1].

## 2.1 Silicon Pixel Detector (SPD)

The SPD plays a key role for the determination of the position of the primary vertex as well as for the measurement of the impact parameter of secondary tracks originating from the

weak decays of strange, charm, and beauty particles. The average distance of the inner SPD layer from the beryllium beam pipe is less than 5 mm.

The SPD is based on hybrid silicon pixels, consisting of a two-dimensional sensor matrix of reverse-biased silicon detector diodes bump-bonded to readout chips.

The detector element, called ladder, is made of one sensor matrix of 256 x 160 pixel cells bump bonded to 5 ALICE1LHCb front-end chips. The pixel cell measures  $50\ \mu\text{m}$  ( $r\phi$ ) by  $425\ \mu\text{m}$  ( $z$ ). The thickness of the sensor is  $200\ \mu\text{m}$ , the smallest that can be achieved with an affordable yield in standard processes, while the thickness of the readout chip is  $150\ \mu\text{m}$ . The two layers SPD barrel contains in total 240 ladders and 1200 chips for a total of  $9.8 \times 10^6$  cells.

The total power dissipated in the SPD front-end electronics is  $\approx 1.35\ \text{kW}$ . The cooling system is of the evaporative type and is based on  $\text{C}_4\text{F}_{10}$ . The reduced performance of the cooling system is limiting the number of modules that can be operated. The temperature of the half-stave is monitored by two Pt1000 chains embedded in the top layer of the pixel module. The power supply system is hard-wired interlocked with the temperature monitoring to protect the SPD in the event of a cooling failure because the temperature would increase at a rate of  $1\ \text{°C/s}$  due to its very low mass.

The SPD front-end electronics readout runs at 10 MHz clock frequency. Each chip is readout in 256 clock cycles, 10 chips are grouped together and constitute the detector module. The two layer SPD barrel comprises 120 detector modules, called half-staves. The 10 chips of each half-stave are readout sequentially in  $256\ \mu\text{s}$ . The same time is required for the full SPD because the 120 half-staves are readout in parallel.

The SPD data stream includes a digital signal (Fast-OR) promptly asserted by each of the 1200 front-end chips when one or more cells in the matrix detect a signal above threshold. This unique capability among the LHC vertex detectors allows the SPD to contribute to the first level trigger decision, improving event selection and background rejection both in p-p and Pb-Pb collisions. Fig. 1 shows a simplified diagram of the interconnections between the SPD readout electronics and trigger and the ALICE Central Trigger Processor [3]. The readout data fibers coming from the detector are connected to 120 passive optical splitters. One of the output branches forwards data to the readout electronics while the second one is connected to the Pixel Trigger System. This is totally decoupled from the readout electronics. The amount of data transmitted by the SPD is of 76.8 Gb/s during readout and of 38.4 Gb/s during idling. The bandwidth of the Fast-OR data is of  $120 \times 10\ \text{bits} \times 10\ \text{MHz} = 12\ \text{Gb/s}$ . The Pixel Trigger System extracts the Fast-OR signals from the data stream and processes them with a fixed latency inside a FPGA, delivering the results to the Central Trigger Processor. The overall latency of these operations is 830 ns. Various trigger algorithms can be implemented and processed in parallel and the future evolution of the trigger algorithms is supported by reconfiguring the processing FPGA from the control room. The result of each of the algorithms, updated every 100 ns, is a single bit trigger primitive. Up to ten primitives are transmitted simultaneously to the ALICE Central Trigger Processor where they can contribute to the first level trigger decision. The total output bandwidth of the Pixel Trigger System is 100 Mb/s.

For the proto-proton interactions program the Pixel Trigger System allows to implement minimum bias trigger conditions, improving background rejection. Moreover, trigger conditions

for rare events based on high multiplicity and on topological conditions (jets) are possible. Selection of events with large impact parameter using the Pixel trigger is foreseen for the research program with heavy ion collisions. All of the algorithms that have been investigated until now are based on multiplicity or topology of Fast-OR signals [3].

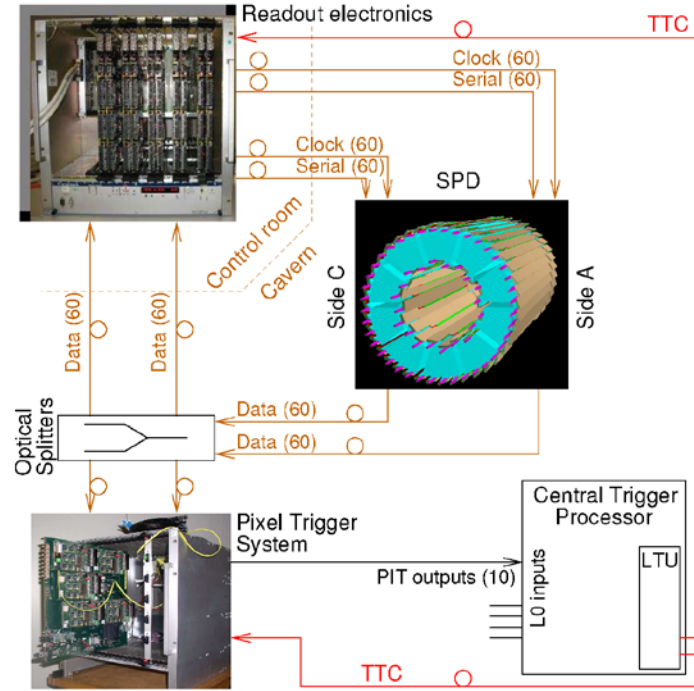


**Figure 1:** Simplified diagram of the interconnections of the SPD trigger system.

## 2.2 Silicon Drift Detector (SDD)

The **SDD** comprises the two intermediate layers of the ITS, where the charged particle density is expected to reach up to 7 per  $\text{cm}^2$ . ALICE is the unique active high energy physics experiment using silicon drift detector for tracking purpose, this is possible because it was optimized for the expected running conditions of LHC with heavy ion beams.

The 260 modules constituting the two-layer SDD barrel are mounted on linear structures called *ladders*. The SDD module consists of one silicon drift detector, produced from very homogeneous high-resistivity ( $3 \text{ k}\Omega\text{cm}$ )  $300 \mu\text{m}$  thick Neutron Transmutation Doped (NTD) silicon, and two front-end hybrids, each connected to the corresponding end-ladder low voltage board.

The sensitive area of the detector module is  $70.17 \times 75.26 \text{ mm}^2$  and it is split into two drift regions by the central cathode strip to which a nominal high voltage bias of  $-1.8 \text{ kV}$  is applied.

The electrons produced by traversing ionizing particles move in opposite directions in the two drift region of a detector and they are collected by an array of 256 anodes of  $294 \mu\text{m}$  pitch located at the end of each drift region.

Moreover, three rows of 33 MOS charge injectors ( $20 \times 100 \mu\text{m}^2$  each) are embedded in each drift region to inject a charge in known positions for monitoring the drift velocity, because

it depends on temperature ( $v_{\text{drift}} \propto T^{2.4}$ ). The electron drift velocity at the nominal electrical field is  $\approx 6.5 \mu\text{m/ns}$  and for calibration the injectors are triggered at regular intervals during the data-taking. The first stage of the SDD front-end electronics is an amplifier-shaper with a peaking time of 40 ns and a dynamic range of 32 fC, corresponding to the charge released by an 8-MIP particle hitting near the anode. The output is sampled at 20 or 40 MHz by a ring analogue memory with 256 cells per anode. The event size is reduced by more than one order of magnitude from the raw 24.4 MB and then transmitted to the VME boards, housed in the counting room, interfacing the detector with the ALICE DAQ system.

The cooling system of the SDD layers has to provide a temperature stability of 0.1 K. The cooling system is a combination of two independent under-pressure water circuits, one coupled to the front-end electronics via the pipes running along the ladders and the other coupled to the readout electronics, LV and HV boards via pipes embedded in the end-ladder structure.

### 2.3 Silicon Strip Detector (SSD)

The SSD comprises the two outermost layers of the ITS, which are crucial for the matching of tracks from the TPC to the ITS.

The detector modules consist of one double-sided sensor each, connected to two hybrids with six front-end chips HAL25 each. The modules are assembled on ladders of the same design as those supporting the SDD. These ladders are one module wide and up to 25 modules long along the beam direction. The SSD layers are made of 72 ladders, carrying a total of 1698 modules. The modules are cooled by water running through two thin, 40  $\mu\text{m}$  wall thickness, phynox tubes along each ladder. The detector modules are 300  $\mu\text{m}$  thick and they have 768 strips on each side with a pitch of 95  $\mu\text{m}$ . The stereo angle is 35 mrad which is a compromise between stereo view and reduction of ambiguities resulting from high particle densities.

The HAL25 front-end chip includes 128 analogue channels. Each channel has a preamplifier to convert the positive or negative charge input from the sensor into an analogue voltage step whose magnitude is proportional to the charge. Its input range is about 300 000 electrons, corresponding to about 14 MIPS in this set-up. The preamplifier is followed by a shaping circuit whose shaping time is remotely adjustable between 1.4  $\mu\text{s}$  and 2.4  $\mu\text{s}$ . The analogue peak value is stored in a sample and holds circuit and then shifted out serially through an integrated analogue multiplexer at a maximum speed of 10 MHz. For testing purposes the HAL25 contains an internal pulser and boundary scan registers. The main task of the FEROM is to digitize the 2.6 million analogue samples from the front-end modules, keeping up with the trigger rate in ALICE.

The average power dissipated inside the barrel is 2.2 kW of which one third in the detector modules. The actual power depends mainly on the readout rate. Each ladder has two cooling pipes operated in counter flow with the EndCap in series with the return on its side. The power supplies are interlocked with temperature sensors on each EndCap. The water system is designed as a leak proof system; it operates below atmospheric pressure. A moderate air flow is provided to even out moisture and temperature gradients inside the SSD volume.

### 3. Commissioning and cosmic runs

In June 2007 the ITS was installed in the ALICE experimental area at Point 2 in the LHC ring. Connection to services (power cables, optical fibres and cooling pipes) could first be done in November 2007, when the mini-frame carrying the service interfaces was lowered and installed in place. A first commissioning run was performed already in December 2007 in order to test the data acquisition and the calibration strategy on a fraction of modules for which power supplies and cooling power were available. The deployment of services was completed in May 2008 as well as the integration of the SPD Fast-OR trigger system with the ALICE Central Trigger Processor.

The unique trigger capability of the SPD has been extensively exploited for the commissioning with cosmic rays and proton beams of the ITS and several other ALICE detectors. The cosmic events were selected by requiring at least one hit in the outer layer of the top half-barrel in coincidence with at least one hit in the outer layer of the bottom half-barrel. The cosmic trigger rate ranged from 0.09 Hz to 0.12 Hz depending on the number of active SPD modules, well in agreement with the Monte Carlo simulations. The purity of the cosmic trigger has been proven to be  $\sim 99.5\%$ .

Data samples of more than  $65 \times 10^3$  events with at least 3 hits in the SPD and more than  $35 \times 10^3$  with at least 4 hits have been collected and were used for the internal alignment of the ITS modules and the ITS with respect to the TPC; moreover the charge signal was calibrated in the SDD and the SSD. The ITS standalone tracking was adapted to reconstruct the cosmic rays as two back-to-back tracks starting from a pseudo-vertex along the cosmic ray trajectory built from the points of the two SPD layers. A detailed description of the alignment procedure and the latest results with the available statistics can be found in [4]. For the SPD modules which had sufficient exposure to the mostly vertical cosmic ray flux, the space point resolution in  $(r, \phi)$  is  $\approx 14 \mu\text{m}$ , to be compared to about  $\approx 11 \mu\text{m}$  obtained from the Monte Carlo simulation without misalignments. For all six layers, the completion of the alignment for all modules requires tracks from proton-proton collisions; a few  $10^6$  events should allow achieving an alignment precision close to the target over the entire detector.

#### 3.1 Silicon Pixel Detector (SPD)

The final integration and full pre-commissioning of the SPD was performed on surface before the installation in ALICE, using the final cooling plant and a full-scale configuration of power supplies, interlock and central systems such as data-acquisition and trigger. This strategy was invaluable for debugging the system before installation in the experimental area.

After the installation, the first phase of the commissioning was based on the use of the on-chip programmable amplitude pulse to verify and optimize the detector functionality. The front-end electronics configuration was tuned by mean of several 8-bit DACs embedded in the front-end chip; the main parameters to optimize being the current and voltage references, the trigger delay, the global voltage threshold and the leakage current compensation. The SPD was initially configured according to the results of the pre-commissioning which allowed recording the first cosmic tracks on 21th February 2009 (see Fig. 2) [5].

In April 2008 the SPD trigger system was installed and commissioned. Since then the SPD has provided a trigger signal extensively used for the commissioning and the data taking for alignment of several detectors as well as for monitoring the beam activity in LHC, as described in the following.

A reduced efficiency of the cooling system has been observed in certain detector areas. The temperature rises locally to values exceeding the safe limits, and the half-staves concerned cannot be continuously powered. The outcome of the in depth investigation indicated a lack of cooling fluid underneath some half-staves; this could be due to impurity clogging in some particulate sintered filters, placed in a region which is unfortunately not accessible at this moment due to the peculiar ALICE layout. The unfavorable thermodynamic condition, which may also cause a degradation of the cooling performance, due to an earlier evaporation of the  $C_4F_{10}$  before it reaches the detector, was ruled out by sub-cooling the  $C_4F_{10}$  close to the detector entrance. In parallel actions to improve monitoring and control of the whole system have been taken. About  $\approx 83\%$  of the detector could be steadily operated during the cosmic rays and beam runs, corresponding to 100 half-staves out of 120 and 1000 front-end chip out of 1200. In the following, all results are referred to this fraction of the detector, unless otherwise specified.

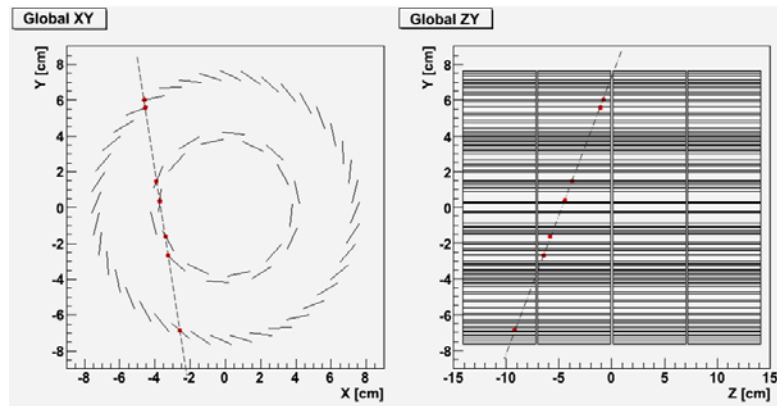


**Figure 2:** SPD online event display used during the cosmic run: side view on the left and view along z on the right. The SPD recorded data in self-triggering mode with a coincidence of top outer and bottom outer layer.

During the commissioning with cosmic rays a re-tuning of the DACs was performed with the aim to find the best compromise between power consumption and detector performance in terms of response uniformity of the pixel matrix, minimum working threshold and number of noisy pixels. The matrix uniformity and the minimum threshold are optimized by injecting a pulse signal of known amplitude generated by the on-chip pulser. The noisy pixels are detected by looking at the pixels firing with a random trigger once the threshold has been fixed. Fig. 3 shows on the left the power consumption and on the right the temperature distributions of the 100 half-staves used for data-taking. The half-stave working temperature is measured by the PT1000 chains embedded on the top surface: the average temperature is  $\approx 30$  °C. It should be noticed that this value is a few degree above the design temperature. This behaviour is again consequence of the limited available cooling power. Despite the cooling system was designed to be well oversized with respect to the expected needs, the overall performance are not fully

satisfactory. The proper actions will be taken during the next long shutdown, meanwhile the monitoring and the tuning of the working conditions have been extensively improved and in particular the flow of the cooling fluid is continuously recorded. The flow turned out to be the key parameter for the operation of an evaporative cooling system, from which one can infer the amount of power that can be removed, although the regime of the fluid inside the circuitry cannot be unambiguously easily established.

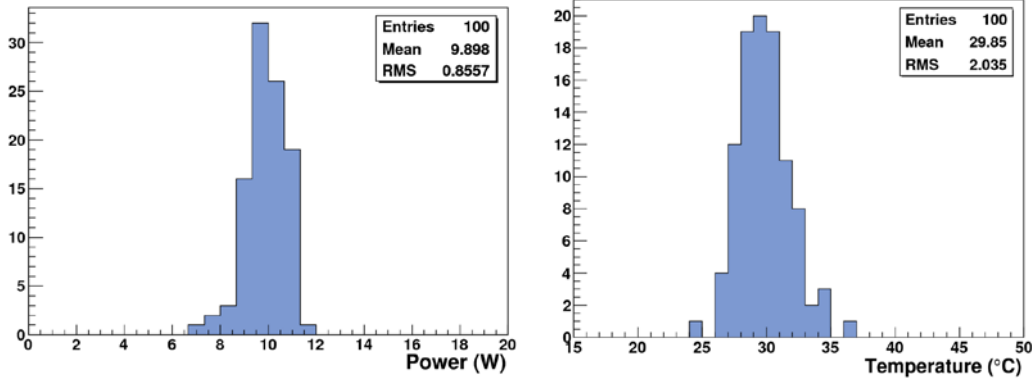


**Figure 3:** Half-stave power consumption (left) and temperature distributions (right).

Fig. 4 shows the front-end chip threshold distribution on the left and the efficiency as a function of the threshold for perpendicular incident tracks from test beam data analysis is shown on the right [6].

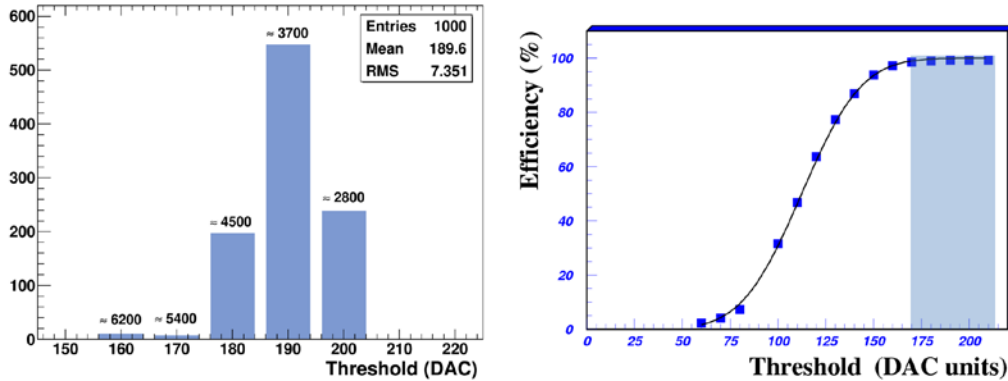


**Figure 4:** Threshold distribution (left) and efficiency as a function of the threshold for perpendicular incident tracks from test beam data analysis (right).

The overall number of dead and noisy pixels is  $< 0.15\%$ . The noisy pixels are masked in the electronics.

The detector readout time has been proven to be  $\approx 300\ \mu\text{s}$ , very well in agreement with the design value, and very slightly dependent on the occupancy well above the expected occupancy. The four-position multi-event buffer embedded in the front-end chip allows a 0% dead-time up to a  $\approx 3\text{kHz}$  trigger rate; the dead time increases at higher rate depending on the probability to

fill an empty slot of the multi-event buffer. At 40 MHz the dead time becomes  $\approx 300 \mu\text{s}$ , corresponding to a maximum readout rate of  $\approx 3.3 \text{ kHz}$  with 100% dead time.

The Fast-OR circuitry is controlled by four DACs which are tuned chip-by-chip in order to time the individual signals, maximize the trigger efficiency and minimize the residual noise. An automatic procedure has been developed to reduce the time needed for this operation. It is based on the use of the on-chip programmable amplitude pulser. An operative setting could be found for a large fraction of the active front-end chip, exactly 927 chips, corresponding to  $\approx 93\%$  out of the 1000 readout and used for tracking. The Fast-OR signals from these chips have been used to define the SPD trigger contribution to the definition of the first level trigger of ALICE. The remaining fraction was excluded by the trigger logic because a satisfactory configuration of the 4 DACs controlling the Fast-OR circuitry could not be found causing the corresponding trigger outputs to be noisy. The flexible design of the pixel trigger system allows easily selecting the chips taking part in the trigger definition and masking the rest.

### 3.2 Silicon Drift Detector (SDD)

The SDD calibration strategy is based on three types of standalone runs collected periodically, typically every  $\sim 24$  hours, during the data taking and analyzed by dedicated quasi-online algorithms that store the obtained calibration parameters in the Offline Condition Database (OCDB). This information is then retrieved from the OCDB during the offline reconstruction by automatically selecting the most recent set of calibration parameters for the run being analyzed [7].

The first type of calibration run is the pedestal run which allows to measure for each of the 133k anodes the values of baseline and noise as well as to tag the noisy channels ( $\sim 0.5\%$ ). The baselines are then equalized to a common value in the AMBRA chips. An example of the noise distribution, raw and corrected for common mode, for the 250 modules that were in acquisition is shown in the left panel of Fig. 5. The average and r.m.s. noise values as a function of run number, i.e. time, are shown in the right panel of Fig. 5; the overall range of the plot spans over about 3 months of data-taking. The mean value of  $\sim 2.3$  ADC counts matches with the design value and should be compared with the  $\sim 100$  ADC counts of the charge distribution peak of a cluster produced by a MIP crossing the sensor close to the anodes.

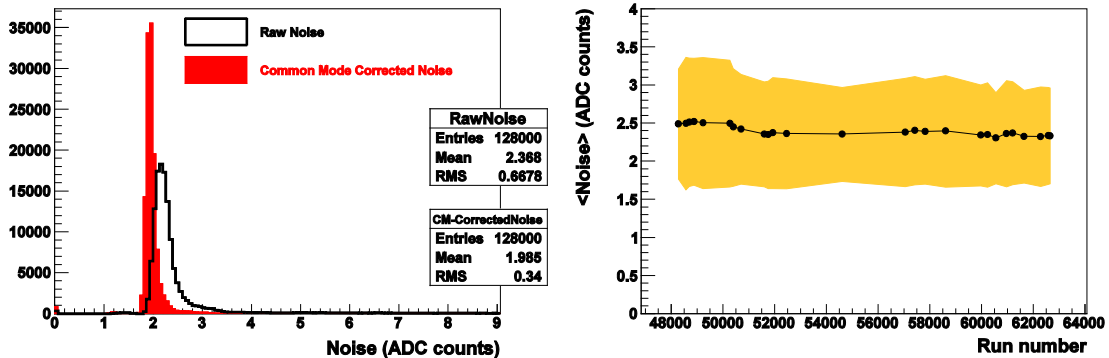


**Figure 5:** The distribution of raw and corrected for common mode noise for all anodes (left) and the average raw noise as a function of the run number (right).

The second type of SDD specific calibration run is the so-called pulse run, where a test pulse is sent to the PASCAL input to measure the channel gain and to tag the dead electronic channels ( $\sim 1\%$ ). The values of gain are used to equalize the signals of the anodes when calculating the spatial coordinates and the total collected charge of the SDD reconstructed points. The distribution of the gain has an r.m.s.  $\sim 4\%$  of the average value, demonstrating a good uniformity of the electronic channels. Also the gain turned out to be stable during 3 months of data taking.

The third type of calibration run is the injector run which provides a measurement of the drift speed in 33 positions along the anode coordinate for each drift region by exploiting the MOS charge injectors. In the left panel of Fig. 6, the drift speed measured by three different anodes of a detector module is plotted as a function of the event number, i.e. time, over a dedicated one hour data-taking. The different values are due to a temperature effect: anodes 16 and 240 are located close to the edge of the sensor where the voltage dividers are located and therefore the temperature is higher and the electron mobility is lower. The r.m.s. average value of the drift velocity fluctuations in one hour are  $\sim 0.07\%$ . The drift speeds of two anodes, one on layer 3 and one on layer 4, as a function of time are shown in the right panel of Fig. 6. The lower drift speed on layer 3 indicates a higher temperature in the inner layer. The higher drift speed values,  $\sim 6.8 \mu\text{m/ns}$ , of layer 4 at the beginning is connected to layer 3 switched off which reflects in a lower temperature on layer 4. In the period with stable detector configuration a remarkable stability, within 1%, of the drift speed on a 2-month time scale is observed.

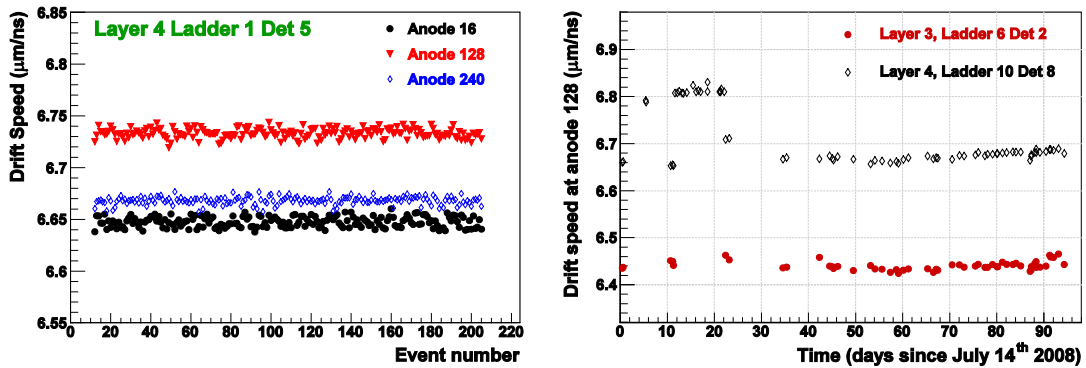


**Figure 6:** The drift speed as a function of the event number in a dedicated one hour run for three anodes of one detector module (left). The drift speed as a function of the time of one anode in each layer 3 and 4 (right).

The alignment of SDD detectors for the coordinate reconstructed from the drift time,  $r\phi$ , is complicated by the interplay between the geometrical misalignment, the calibration of drift speed and the time zero  $t_0$ , which is the measured drift time for particles with zero drift distance. The  $t_0$  parameter accounts for the delay between the time a particle crosses the detector and the arrival time of the trigger signal. Two methods have been developed in order to obtain a first estimate of the  $t_0$  parameter. The first and simpler method consists in extracting the  $t_0$  from the minimum measured drift time on a large statistics of reconstructed SDD points: the distribution of measured drift times is built and the sharp rising part of the distribution at small drift times is used to extract the  $t_0$  with an ad-hoc fitting function. The second method measures the  $t_0$  from the residual distributions along the drift direction between tracks fitted in SPD and SSD layers

and the corresponding points reconstructed in the SDD. These distributions, in case of miscalibrated  $t_0$ , show two opposite-signed peaks corresponding to the two drift regions of each SDD module where electrons move in opposite directions. The  $t_0$  can then be calculated from the distance of the two peaks and the drift speed.

The atmospheric muons provide also a sample of ionizing particles for absolute calibration of the  $dE/dx$ . In case of SDD detectors, the collected charge actually depends on drift distance due to the applied zero-suppression: the larger the drift distance, the larger the charge diffusion and consequently the electron cloud develops wider tails which get more easily cut by the zero-suppression algorithm. This effect is shown in the left panel of Fig. 7, where the cluster charge distribution in two intervals of measured drift time is reported for a sample of atmospheric muon tracks collected without magnetic field. The distributions are fitted with a convolution of a Landau and a Gaussian.

In the right panel of Fig. 7, the Most Probable Value (MPV) of energy deposit extracted from Landau-Gaussian fit in seven bins of drift time is plotted as a function of the drift time. The MPV decreases with increasing drift time. By applying to the reconstructed cluster charge the correction for the combined effect of diffusion and zero-suppression thresholds, which is extracted from detailed simulations of the detector response, the MPV results to be independent of drift time, as it can be seen from the open triangle points in the right panel of Fig. 7.

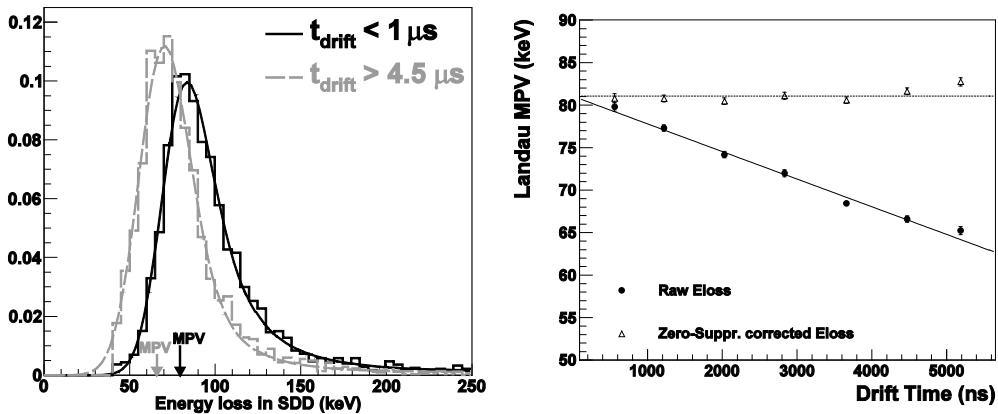


**Figure 7:** Distribution of energy loss for points reconstructed in the SDD detector for two intervals of drift time; fits with a convolution of a Landau and a Gaussian are superposed (left). The Most Probable Value vs. drift time, with and without correction for zero-suppression effect (right).

It should be noted that electron trapping during the drift may also induce a charge dependence on drift time similar to the one observed in Fig. 7. Since these trapping effects are not included in the Monte Carlo simulations used to extract the applied correction, we can conclude that the observed charge dependence on drift time is mainly due to the effect of the thresholds applied by the zero-suppression algorithm. This has also been confirmed by measurements performed in the laboratory on few spare SDD modules, where no dependence of cluster charge on drift time was observed when the zero-suppression was disabled [7].

### 3.3 Silicon Strip Detector (SSD)

The SSD commissioning of the installed detector was done in two steps, first in “*standalone mode*” and later in “*global mode*” cosmic runs, i.e. taking data together with the other ITS detectors [8]. The first steps were standalone runs with the full detector powered on to validate and tune the SSD components; standalone runs with a free-running pulser trigger were taken to study noise and optimize the bias voltages for each half-ladder. Since common-mode shift is the main contribution to the total correlated plus uncorrelated noise, a correction for common mode signals was implemented in the firmware of the read-out electronics, thus resulting in an almost ten-fold reduction of the noise in the raw data and consequently a reduction in the data volume by suppression of empty data channels. Further tuning of the detector enabled recovering part of the declared bad ladders, either modules or individual strips, while maintaining the low level of noise hits. After the fine tuning, the overall fraction of the detector that could be operated was 90%. The following steps were the timing adjustment, calibration of the charge deposition measurement and the software alignment of the modules, as described in the following.

Particles crossing the sensor create electron-hole pairs, which are collected by the implanted strips forming a sharp impulse of charge. The HAL25 front-end chip integrates the charge with a shaping time of  $2.2\mu\text{s}$  and the output of the shaper is then stored in an integrated capacitor upon receiving an HOLD signal. The read-out and digitalization electronic FEROM is placed in the rack, about 30m apart from the detector, and for a proper operation of the detector, two types of time adjustment are needed: read-out clock synchronization and HOLD timing.

At the read-out start time, the FEROM generates a token which is sent to the first chip of the module and propagates at 10 MHz clock rate through the 1536 channels of the 12 daisy chained HAL25. The token triggers the transfer of the stored value to the differential pair analog bus. The module signal is thus appearing as a sequence of 1536, 100ns wide, analogue levels. The time between sending the token and the start of digitization in the FEROM has to be adjusted to take into account the signal transit time over the cables between the FEROMs and the ladders. The sampling should happen in the centre of the interval, to be immune from small jitters and from the smoothing appearing in the passage between the values of two consecutive strips. If this timing is not set appropriately the signal will be associated to the wrong strip position, resulting in a kind of “misalignment” of the detector or if the sampling is happening in the transition region, a mis-evaluation of the signal ( $\sim$ double counting).

The HAL25 front-end amplifier allows choosing the shaping time in the range 1.4- $2.2\mu\text{s}$ . The nominal value of  $2.2\mu\text{s}$  has been chosen for the data taking. To achieve the maximum signal to noise ratio and the signal stability against small jitter of the trigger arrival time, the signal should be sampled on the flat top of the shaping curve. For this reason the HOLD signal should reach the HAL25  $2.2\mu\text{s}$  after the particle has crossed the sensor, with a precision of some tens of ns. The plot of the Most Probable Values (MPV) as a function of the L0 trigger delay within the span of  $4\mu\text{s}$  available in the FEROM is shown in Fig. 8. The detector working configuration is selected to correspond to the maximum of this plot.

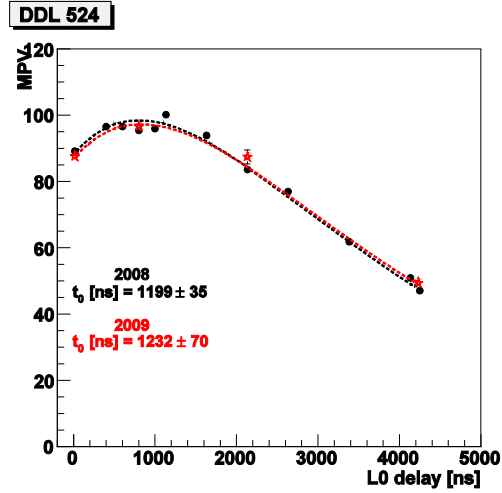


Figure 8: The MPV extracted from the Landau fits as a function of the L0 trigger delay.

The response of a double-side detector to the energy released by the crossing particle can be split in two components: relative calibration of the two sides of the detector and an overall conversion of ADC values to energy loss. Both calibrations relied on cosmic muons. The left panel of Fig. 9 shows the charge matching P/N after the relative gain calibration. Only P-N pairs lying along the diagonal, between the two red lines, are considered hits. The right panel of Fig. 9 shows the energy loss measured by the two SSD layers as a function of the particle momenta for one of the first cosmic data sample analyzed [8].

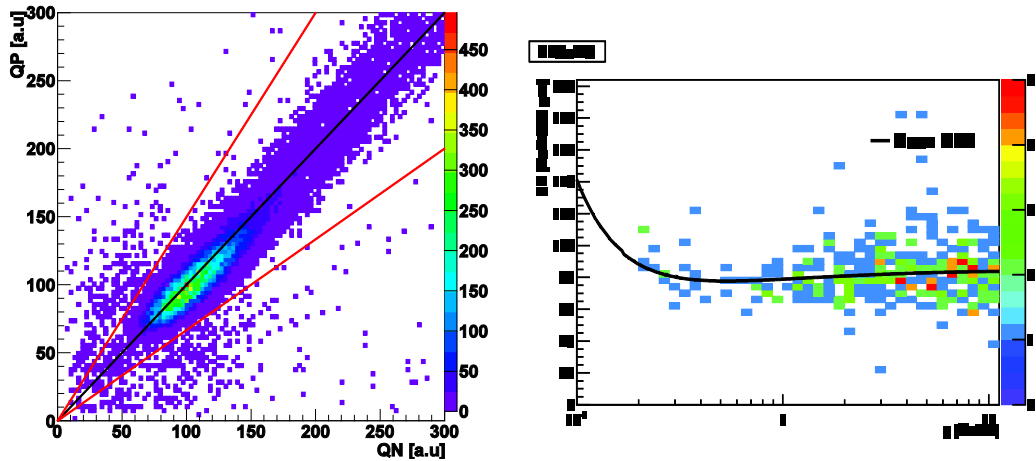
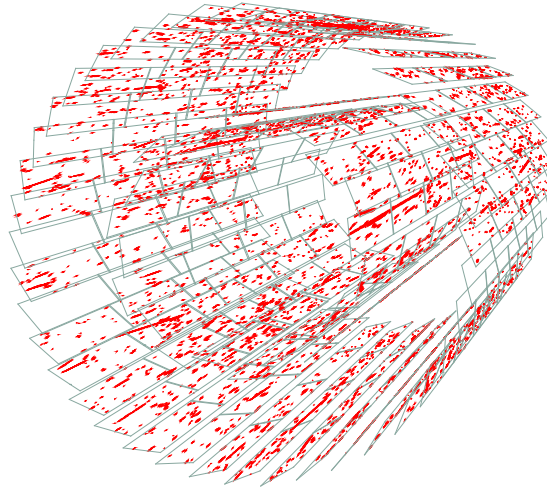


Figure 9: Cluster charge of P-side vs. N-side, the two red lines show the position of the cuts used in the charge matching (left) and the  $dE/dx$  distribution as a function of the particles momenta for cosmic tracks (right).

#### 4. Experience with beams

Since the beginning, the ITS commissioning plan aimed to be ready by the time that the LHC would have delivered the first proton-proton collisions, which in an early stage was expected to happen in autumn 2008. The ITS and in particular the SPD is one of the ALICE sub-detectors contributing to the measurement of the charged-particle multiplicity, which is the common objective of “day-one” studies for all the LHC experiments. Indeed, the

commissioning was well advanced when on the evening of 15 June 2008, while preparing the ITS for the usual cosmic run, the triggered event from the SPD showed a puzzling pattern in the two SPD layers, never seen before. The recorded events contained long straight tracks developing parallel to the beam axis for several centimetres in the active volume of the 200  $\mu\text{m}$  thick silicon sensors, an example of such event is shown in Fig. 10. Some tracks in these events crossed the gaps between adjacent sensors and adjacent readout chips. They were the muon tracks produced in the proton beam dump during an injection test in the transfer line close to the ALICE cavern: this was the first sign of life of LHC detected by an experiment [9].



**Figure 10:** The first event with particles generated in LHC ever seen by a LHC experiment. The muons generated in the beam dump far away from the ALICE interaction point travel parallel to the beam axis making long tracks in the SPD.

Since then a number of beam injection tests were made at the LHC, including those in the section of the collider preceding the ALICE cavern: the beam was dumped either at the end of the transfer line or just before reaching the ALICE cavern. The SPD was operated in self-triggering mode during all these tests and it provided a valuable information on the beam induced background in ALICE caused by the residual gas in the beam pipe and the insertion in the ring and in the transfer line of the beam monitoring screens: the probing measurement was the raw hit multiplicity detected by SPD, corresponding to an occupancy that locally went up to more than 10%.

In September 2008 the ITS was ready for the LHC star up and indeed on the 10<sup>th</sup>, the day when the beam made the first complete turn of LHC, the SPD was the first detector to light up with particle “debris” created as beam in the transfer line from the SPS hits the beam stop before the ALICE cavern [10]. Another day to remember was the 12<sup>th</sup> of September 2008 when the ITS triggered by the SPD caught the first beam induced interaction ever seen by an LHC experiment.

In October 2008, ALICE entered into shut-down mode for a number of modifications, improvements and maintenance operations to be carried out during the repair period of the LHC. The re-commissioning of the ITS restarted in June/July 2009 as well as the cosmic data taking for calibration and alignment with a without magnetic field. An extensive campaign of test was performed to verify after the long stop the readiness of the ITS in conjunction with the

ALICE Data Acquisition, Detector Control and Central Trigger systems. The various LHC injection tests were used to commission the SPD trigger system and the time alignment of the various ALICE trigger detectors, which benefited from the high purity and time accuracy of the L0 trigger signal provided by the SPD. The SPD L0 trigger has been proved to be reliable and in addition is the fastest contribution to the ALICE L0 trigger definition and therefore it is used as absolute time reference for all trigger detectors. The ITS participated to the ALICE campaign of drill tests aimed to thoroughly debug and verify the readiness of the Physics partition made of selected sub-detectors in conjunction with the ALICE central systems, i.e. data acquisition, central trigger processor, detector control system and high level trigger: the readout time and the event size expected in p-p collisions for all three ITS sub-detectors are reported in Table 2.

**Table 2:** Readout time and event size expected in p-p collisions at nominal occupancy

Detector	Readout time ( $\mu\text{s}$ )	Event size (kB)
SPD	300	5.7
SDD	1023 (20 MHz)	11.1
	2110 (20 MHz)	
SSD	300	84.2

The LHC delivered the first proton-proton collisions just while this paper was being finalized for the proceedings. Although the event took place after this Conference, the author would like to take this opportunity to outline briefly here that exciting experience.

On 23rd November 2009, during the early commissioning of the LHC, two counter-rotating proton bunches were circulated for the first time concurrently in the machine, at the LHC injection energy of 450 GeV per beam. Although the proton intensity was very low, with only one pilot bunch per beam, and no systematic attempt was made to optimize the collision optics, all LHC experiments reported a number of collision candidates. In the ALICE experiment, the collision region was centred very well in both the longitudinal and transverse directions and 284 events were recorded in coincidence with the two passing proton bunches.

For this run about 83% of the SPD modules were operational for particle detection, of which 93% of the chips were used in the trigger logic, about 92% of the SDD anodes and about 90% of the SSD modules were active. The trigger used to record the events was defined by requiring at least two hit chips in the SPD, in coincidence with the signals from the two beam pick-up counters indicating the presence of two passing proton bunches. The intensive commissioning work done to prepare the detector for the first collisions in terms of both tracking and triggering capability, when the LHC started with beams the left over main task was the phase alignment of the internal SPD clock, running at 10 MHz, with the standard accelerator clock at 40 MHz.

These events have been analyzed and the SPD data have been used to measure the pseudorapidity density of charged primary particles in the central pseudorapidity region in the range  $|\eta| < 0.5$ , published in the first physics paper of a LHC experiment [11]. The results have been found to be consistent with previous measurements in proton-antiproton interactions at the same centre-of-mass energy at the CERN SppS collider. They also illustrate the excellent

functioning and rapid progress of the LHC accelerator, and of both the hardware and software of the ALICE experiment, in this early start-up phase and they also establish a reference for comparison with forthcoming measurements at higher LHC energies.

## 5. Conclusion

In this paper we have presented the main results from the commissioning of the Inner Tracking System of the ALICE experiment using cosmic data and the first experience with beams.

The ITS was installed in June 2007 and the commissioning in ALICE was started in December 2007 after the cabling and cooling connections. All the read out electronics and power supplies are in place and commissioned.

Individual detector commissioning and calibration was successfully carried on and the whole ITS took part in cosmic data taking for calibration and alignment purposes with the magnets at various settings. The SPD trigger system was commissioned with the required trigger algorithms; it allows including the Fast-OR outputs in the first level (Level 0) trigger decision of the ALICE experiment. ALICE is the only LHC experiment that includes the vertex detector in the first trigger decision. The read-out time and dead time for the three ITS sub-detectors have been measured and are in agreement with the design specifications.

The pioneering self-triggering functionality of the ALICE SPD proved extremely useful during the testing and commissioning of the detector and later for the entire ALICE experiment. The two key elements enabling this functionality are the pre-processing of trigger primitives on the front-end chips and the availability of large bandwidth data collection and real time processing capabilities on off detector programmable electronics.

So far, about 83% of the SPD modules, of which 93% of the chips were used in the trigger logic, about 92% of the SDD anodes and about 90% of the SSD modules have been operational for particle detection during cosmic rays and beam runs.

The performance of the three silicon detectors of the ITS is shown to be close to the design values. A fraction of the detector modules could not be operated mainly due to the reduced cooling performance and some residual connection problems both optical and electrical. Unfortunately the ALICE layout does not allow to access the ITS unless an heavy dismantling of a considerable part of the experiment. This intervention is compatible with the next long shutdown, which is scheduled for the end of 2011.

The ALICE experiment and in particular the ITS is ready to take data with pp and PbPb collisions to be provided by the LHC accelerator. During the early phase of the LHC commissioning the first proton-proton collisions were observed in ALICE with the ITS detector and they have been used to measure the pseudorapidity density of charged primary particles at  $\sqrt{s} = 900$  GeV in the central pseudorapidity region  $|\eta| < 0.5$ . This result demonstrates that the ALICE experiment has entered the phase of physics exploitation.

## References

- [1] K. Aamodt et al. (ALICE Collaboration), JINST 3 (2008) S08002
- [2] ALICE Collaboration, J. Phys. G **30**, 1517 (2004)

- ALICE Collaboration, J. Phys. G **32**, 1295 (2006)
- [3] G.A. Rinella (ALICE Collaboration), in *Proceedings of 9<sup>th</sup> International Conference on Large Scale Application and Radiation Hardness of Semiconductor Detectors 2009 (RD09), September 2009, Florence, Italy*, PoS(RD09)005
- [4] A. Dainese (ALICE Collaboration), *this Proceedings*  
ALICE Collaboration, J. Instrum. **5**, P03003 (2010)
- [5] R. Santoro et al. (ALICE Collaboration), J. Instrum. **4**, P03023 (2009)
- [6] G.E. Bruno et al., ALICE Internal Note, ALICE-INT 2005-007 (2004)  
G.E. Bruno et al., ALICE Internal Note, ALICE-INT 2005-011 (2005)
- [7] F. Prino (ALICE Collaboration), in *Proceedings of 9<sup>th</sup> International Conference on Large Scale Application and Radiation Hardness of Semiconductor Detectors 2009 (RD09), September 2009, Florence, Italy*, PoS(RD09)007
- [8] P. Christakoglou (ALICE Collaboration) in *Proceedings of the 2009 Europhysics Conference on High Energy Physics (EPS HEP 2009), July 2009, Krakow, Poland*, PoS(EPS-HEP 2009)124
- [9] V. Manzari and G. Stefanini, CERN Courier, Vol. 48, N. 6, July/August 2008
- [10] CERN Courier, Vol. 48, N. 9, November 2008
- [11] K. Aamodt et al. (ALICE Collaboration), Eur. Phys. J. C (2010) 65: 111–125